



Heriot-Watt University
Research Gateway

Inelastic Scattering of CN Radicals at the Gas-Liquid Interface Probed by Frequency-Modulated Absorption Spectroscopy

Citation for published version:

Lane, PD, Moncrieff, K, Greaves, SJ, McKendrick, KG & Costen, ML 2020, 'Inelastic Scattering of CN Radicals at the Gas-Liquid Interface Probed by Frequency-Modulated Absorption Spectroscopy', *Journal of Physical Chemistry C*, vol. 124, no. 30, pp. 16439-16448. <https://doi.org/10.1021/acs.jpcc.0c04023>

Digital Object Identifier (DOI):

[10.1021/acs.jpcc.0c04023](https://doi.org/10.1021/acs.jpcc.0c04023)

Link:

[Link to publication record in Heriot-Watt Research Portal](#)

Document Version:

Peer reviewed version

Published In:

Journal of Physical Chemistry C

Publisher Rights Statement:

This document is the Accepted Manuscript version of a Published Work that appeared in final form in the Journal of Physical Chemistry C, copyright © American Chemical Society after peer review and technical editing by the publisher. To access the final edited and published work see <https://doi.org/10.1021/acs.jpcc.0c04023>

General rights

Copyright for the publications made accessible via Heriot-Watt Research Portal is retained by the author(s) and / or other copyright owners and it is a condition of accessing these publications that users recognise and abide by the legal requirements associated with these rights.

Take down policy

Heriot-Watt University has made every reasonable effort to ensure that the content in Heriot-Watt Research Portal complies with UK legislation. If you believe that the public display of this file breaches copyright please contact open.access@hw.ac.uk providing details, and we will remove access to the work immediately and investigate your claim.

Inelastic Scattering of CN Radicals at the Gas-Liquid Interface Probed by Frequency-Modulated Absorption Spectroscopy

Paul David Lane, Katya E. Moncrieff, Stuart Jeffrey Greaves, Kenneth G. McKendrick, and Matthew L. Costen

J. Phys. Chem. C, **Just Accepted Manuscript** • DOI: 10.1021/acs.jpcc.0c04023 • Publication Date (Web): 07 Jul 2020

Downloaded from pubs.acs.org on July 17, 2020

Just Accepted

“Just Accepted” manuscripts have been peer-reviewed and accepted for publication. They are posted online prior to technical editing, formatting for publication and author proofing. The American Chemical Society provides “Just Accepted” as a service to the research community to expedite the dissemination of scientific material as soon as possible after acceptance. “Just Accepted” manuscripts appear in full in PDF format accompanied by an HTML abstract. “Just Accepted” manuscripts have been fully peer reviewed, but should not be considered the official version of record. They are citable by the Digital Object Identifier (DOI®). “Just Accepted” is an optional service offered to authors. Therefore, the “Just Accepted” Web site may not include all articles that will be published in the journal. After a manuscript is technically edited and formatted, it will be removed from the “Just Accepted” Web site and published as an ASAP article. Note that technical editing may introduce minor changes to the manuscript text and/or graphics which could affect content, and all legal disclaimers and ethical guidelines that apply to the journal pertain. ACS cannot be held responsible for errors or consequences arising from the use of information contained in these “Just Accepted” manuscripts.

Inelastic Scattering of CN Radicals at the Gas-Liquid Interface Probed by Frequency-Modulated Absorption Spectroscopy

*Paul D. Lane, Katya E. Moncrieff, Stuart J. Greaves, Kenneth G. McKendrick and Matthew L. Costen**

Institute of Chemical Sciences, School of Engineering and Physical Sciences, Heriot-Watt University, Edinburgh, EH14 4AS, United Kingdom

ABSTRACT

We describe the results of the first application of frequency-modulated (FM) absorption spectroscopy to molecular scattering dynamics at a gas-liquid interface. A pulsed direct-current electric discharge of a supersonic expansion of BrCN seeded in He was used to generate a pulsed molecular beam of rotationally cold CN($X^2\Sigma^+$) radicals, with a mean laboratory-frame kinetic energy of 43.5 kJ mol⁻¹. The molecular beam was directed at normal incidence onto a continually refreshed perfluoropolyether liquid surface. FM absorption spectroscopy on the CN($A^2\Pi-X^2\Sigma^+$) (2,0) band was used to measure Doppler lineshapes for individual CN rotational states as a function of time after the DC discharge pulse. This enabled the characterization of both the incident molecular beam and inelastically surface-scattered CN rotational and translational energy

1
2
3 distributions. The surface-scattered CN rotational distribution is well-characterized by a single
4 temperature of 850 ± 130 K. The translational distributions perpendicular to the surface normal
5 are non-Maxwellian, and are substantially superthermal. We interpret these observations as the
6 result of *impulsive scattering* being the dominant mechanism, similar to our previous independent
7 measurements of OD inelastic scattering at liquid surfaces. Within the current limitations of signal-
8 to-noise, no clear evidence for a discrete component from *thermal desorption* is observed, in
9 contrast to previous literature measurements of NO and CO₂ scattering at perfluoropolyether
10 surfaces.
11
12
13
14
15
16
17
18
19
20
21
22
23
24
25

26 INTRODUCTION

27
28
29 Interactions between gas-phase molecules and liquid surfaces are common and practically
30 important in a wide range of biological, technological and natural environments. Examples include
31 respiration, distillation, gas separation and sequestration, heterogeneous catalysis and atmospheric
32 aerosols. Experimental investigation of reactive and/or inelastic collisions of gas-phase species
33 with liquid surfaces has lagged behind the equivalent with solid surfaces, generally because of the
34 added difficulties of handling liquids in high-vacuum experiments. More recently, however,
35 scattering at the gas-liquid (G-L) interface has been the subject of increasing experimental
36 investigation.¹⁻³
37
38
39
40
41
42
43
44
45
46
47

48 The majority of experimental studies of G-L scattering have used molecular beam sources to
49 direct the incident atoms or molecules at the surface, ensuring a well-defined collision energy and
50 incident angle, as well as a cold internal state distribution for incident molecules. Two main
51 experimental approaches have been taken to detect the gas-phase products of scattering. Mass
52
53
54
55
56
57
58
59
60

1
2
3 spectrometric detection has the substantial advantage of ‘universality’, and is well suited through
4
5 time-of-flight measurements to the determination of product translational energy distributions, and
6
7 if implemented with rotation of the detector assembly, to measurement of angular scattering
8
9 distributions.¹⁻⁵ However, it does not provide resolution of the product quantum-state distribution.
10
11 The alternative approach, first demonstrated for inelastic scattering of I₂ by McCaffery and co-
12
13 workers,⁶⁻⁷ and subsequently developed and extensively applied in our own laboratory,⁸⁻¹⁷ and
14
15 separately by Nesbitt and co-workers,¹⁸⁻³³ is to use laser spectroscopic techniques. These are
16
17 inherently quantum state specific, but do not provide speed and angular information in such a
18
19 straightforward fashion.
20
21
22

23
24 Our previous work has used laser-induced fluorescence (LIF) to detect OH(D)(X²Π) radicals,
25
26 either as the reactive product of O(³P/¹D) scattering at liquid surfaces containing alkyl groups, or
27
28 as the direct result of inelastic scattering of OH(D) from inert and reactive surfaces. This detection
29
30 technique has been coupled to both photolytic generation of the reactive O or OH directly above
31
32 (typically 10 mm) the liquid surface, and to molecular beam sources of OH(D).¹⁶ With photolytic
33
34 and molecular beam sources of OH(D), we have determined reactive sticking coefficients for
35
36 OH(D) at saturated and unsaturated hydrocarbon surfaces, together with ro-vibrational product
37
38 state distributions for OH(D) inelastic scattering at reactive hydrocarbon and inert surfaces.^{9, 16, 34}
39
40 Using photolytic generation we have studied reactions of O(³P) or O(¹D) at saturated and
41
42 unsaturated hydrocarbon surfaces, determining ro-vibrational product state distributions as well as
43
44 information on the translational energy distributions of these products.^{8, 10, 12, 14} We have used our
45
46 understanding of O(³P) reaction dynamics at hydrocarbon surfaces, arising from these dynamical
47
48 studies of reactive and inelastic scattering, to develop reactive atom scattering (RAS) as a probe
49
50 of the hydrocarbon density at the liquid surface, and have applied it to understanding the interfacial
51
52
53
54
55
56
57
58
59
60

1
2
3 chemical structure of a wide range of ionic liquids and ionic-liquid mixtures.^{11, 13, 15} Most recently,
4 we have extended this methodology to real-space LIF imaging, expanding the probe laser beam to
5 a sheet intercepting both the in-going OH molecular beam, and out-going scattered OH. Imaging
6 of the fluorescence in the plane containing the molecular beam and the surface normal as a function
7 of time after the OH is incident on the surface provides a real-space measurement of the scattering
8 dynamics for a single ro-vibrational state, enabling correlated angular and translational energy
9 information to be determined.¹⁷

19 Nesbitt and co-workers have also used LIF to detect the products of inelastic scattering at G-L
20 interfaces, specifically NO ($X^2\Pi$) scattering from ionic liquids and liquid metals,^{28-30, 32} and
21 desorbing from an aqueous microjet.³³ More significantly for the work presented here, they have
22 also demonstrated the application of direct high-resolution laser absorption spectroscopy in the
23 mid-IR for the detection of the products of G-L scattering. In a wide range of experiments, this has
24 included HF formed as a product of reactive scattering of F(2P) at a saturated hydrocarbon
25 surface,^{20, 25} and extensive measurements of the dynamics of inelastic scattering, particularly of
26 CO₂, at a range of liquid surfaces.^{18-19, 21-24, 26-27} Absorption spectroscopy is generally less sensitive
27 than LIF, and enhancing sensitivity requires long path lengths, resulting in much lower spatial
28 sensitivity than LIF. However, a fundamental advantage is the ability to probe many species that
29 are inaccessible to LIF, because they lack suitable fluorescent excited electronic states. This is the
30 case for many closed shell species, such as HF and CO₂. In contrast, essentially all molecular
31 species outside homonuclear diatomics exhibit vibrational transitions that are accessible via IR
32 absorption spectroscopy. Another advantage of IR laser absorption spectroscopy is that it is
33 conventionally performed with continuous wave (cw) lasers. When combined with pulsed
34 generation of the incident atoms or molecules this enables a complete measurement of the
35
36
37
38
39
40
41
42
43
44
45
46
47
48
49
50
51
52
53
54
55
56
57
58
59
60

1
2
3 appearance time of the scattered products, and hence information on the translational energy of the
4 scattered products, to be determined on every repetition. This results in a duty cycle improvement
5 over conventional LIF with pulsed lasers, where the delay between generation and probing must
6 be scanned in a sequential fashion. The narrow spectral bandwidth of most cw-lasers also allows
7 high-resolution Doppler spectroscopy of individual ro-vibrational transitions, and the consequent
8 measurement of the projection of the molecular velocity distribution onto the laser-propagation
9 axis, which is generally perpendicular to the surface normal. Such Doppler spectroscopy is not
10 easily achievable in LIF with conventional pulsed dye lasers, as their typical spectral bandwidths
11 are similar to the measured Doppler widths.
12
13
14
15
16
17
18
19
20
21
22
23

24 In this paper, we demonstrate the first application of frequency-modulated (FM) transient
25 absorption spectroscopy to gas-liquid scattering. FM absorption spectroscopy has been widely
26 used as a sensitive spectroscopic method,³⁵⁻³⁶ which has been applied previously to probe gas-
27 phase photodissociation dynamics,³⁷⁻³⁸ reaction kinetics,³⁹⁻⁴⁰ and collisional energy transfer
28 dynamics.⁴¹⁻⁴² The first allowed electronic transition of the cyanogen radical, $\text{CN}(A^2\Pi-X^2\Sigma^+)$,
29 occurs in the near-infrared, convenient for many commercially available narrow-band continuous-
30 wave laser sources. This makes it an excellent target species for transient FM spectroscopy. In our
31 laboratory, we have previously applied FM spectroscopy to study the dynamics of gas-phase
32 collisional energy transfer of both $\text{CN}(X^2\Sigma^+)$ and $\text{CN}(A^2\Pi)$ radicals.⁴³⁻⁴⁹ In this paper, we combine
33 the sensitive FM absorption detection with a new pulsed molecular beam source of $\text{CN}(X)$ radicals
34 to study the inelastic scattering of $\text{CN}(X)$ at an inert perfluoropolyether (PFPE) liquid surface.
35
36
37
38
39
40
41
42
43
44
45
46
47
48
49
50
51
52
53
54
55
56
57
58
59
60

EXPERIMENTAL METHODS

Experiments were performed in a newly constructed vacuum apparatus (Fig. 1), consisting of molecular beam source and liquid-surface scattering chambers, separated by a removable bulkhead. The source and scattering chambers were evacuated by turbomolecular pumps (Edwards nEXT400D and nEXT300D respectively), which were backed by a dry scroll pump (Edwards XDS 10iC), providing a base pressure of ca. 10^{-8} mbar.

A molecular beam of CN(X) radicals was produced by a pulsed DC electric discharge of BrCN (Sigma-Aldrich 97%) diluted to a mole fraction of 0.4% in He carrier gas (BOC gases, CP grade 99.999%, total pressure 3 bar) at the exit of pulsed valve (Parker series 9, 1 mm aperture). We have previously described the design of the electric discharge system in application to production of an OH(X²Π) molecular beam.¹⁶ The high voltage pulse, nominally a square wave with rise and fall times of ≈ 10 ns, was produced by a circuit based around a commercial push-pull fast switch (Behlke HTS-41-06-GSM). This was externally triggered to switch between ground and the optimized discharge voltage of -2000 V for a period of 10 μ s, ~ 100 μ s into a gas pulse of nominal overall length 260 μ s. These timings were controlled by a digital delay generator (Stanford Research Systems DG535). The optimized voltage was established by monitoring both the CN FM signal size (vide infra) and the shot-to-shot stability of the discharge. The stability was improved by seeding with electrons emitted from a hot tungsten filament (Agar Scientific A054, $I = 2.6$ A, $V = 15 - 20$ V), positioned in the line of sight of the discharge, ~ 2 cm in front and ~ 2 cm to the side of the exit of the discharge.⁵⁰ Without the filament, discharge stability varied from day-to-day, with failure to strike on up to 30% of shots. With the filament consistent operation was achieved, with $< 1\%$ of shots missed. Discharge stability was also found to improve at lower

1
2
3 repetition rates of the pulsed valve, and a balance between this and the duty cycle resulted in the
4
5 selection of 5 Hz for the experiments presented here.
6
7

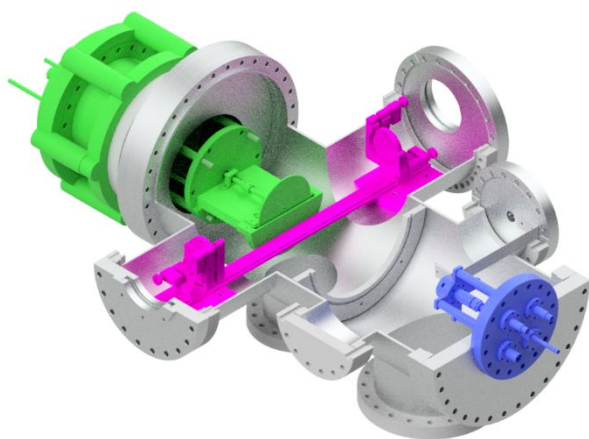
8
9 The CN molecular beam was directed, parallel to the surface normal, at a continuously-refreshed
10
11 liquid surface, generated by the well-established rotating-wheel method.²⁻³ The PFPE (Krytox
12
13 1506 (F-[CF(CF₃)CF₂O]_{14ave}-CF₂CF₃), Dupont) was contained within a copper bath. The
14
15 temperature of the bath was controlled by a heater/chiller (Cole-Parmer Polystat WZ-12122-34)
16
17 with an operating range of -28 to 100°C. In the work presented here, all measurements were
18
19 performed at 25°C, where the vapor pressure of PFPE is $\approx 10^{-7}$ mbar. A 10 cm diameter stainless-
20
21 steel wheel was partially submerged in the PFPE. The wheel rotated at 0.5 Hz and was
22
23 consequently coated in a continually refreshed layer of the liquid. The wheel-bath assembly was
24
25 mounted on a heavy-duty in-vacuum z-translator (LewVac M-HDZ101-160CF), enabling it to be
26
27 either positioned in line with the probe Herriott cell (vide infra) or retracted by 10 cm, to enable
28
29 measurements on the incident molecular beam without surface-scattering interference. The
30
31 molecular beam source was operated as a free-jet expansion, positioned 317 mm from the wheel,
32
33 and directed at a spot on the wheel 25 mm above the axis of rotation and horizontally centered.
34
35 The radius of the expansion at the surface was estimated from analysis of the Doppler lineshape
36
37 for $j = 0.5$ to be ≈ 100 mm. Under operating conditions, with the PFPE and the molecular beam
38
39 present in the chamber, the average pressure was $2-5 \times 10^{-5}$ mbar.
40
41
42
43
44
45

46
47 CN was probed using frequency-modulated transient absorption via R₁ branch lines of the A²Σ⁺-
48
49 X²Π (2,0) band between 778 and 795 nm. The FM probe system has been described in detail in
50
51 several previous publications, and only the essentials are presented here.^{43, 45, 48} The output of a
52
53 single mode external-cavity tunable diode laser (Sacher GmbH TEC520) was frequency modulated
54
55 at 400 MHz using a broadband phase modulator (Quantum Technologies, TWAP-10). A
56
57
58
59
60

1
2
3 wavemeter (Angstrom WS-6) and a scanning Fabry-Perot interferometer were used to monitor the
4
5 frequency modulation and provide an accurate wavelength scale. The laser beam was multi-passed
6
7 parallel to the liquid surface in a Herriott cell located inside the vacuum chamber. The Herriott cell
8
9 was of the design of Kaur et al,⁵¹⁻⁵² using mirrors (Thorlabs CM508-100-E03, reflectivity $R \geq$
10
11 0.995 from 750 to 1100 nm, radius of curvature, $r = 20$ cm) separated by 40.1 cm. The beams
12
13 converged on the center of the cell, forming a circle of ~ 8 mm diameter with 14 passes that gave
14
15 a total path length within the Herriot cell of ≈ 5.6 m, at a nominal distance of 20 mm from the
16
17 surface of the wheel. The output was passed to a 1 GHz photoreceiver (NewFocus 1601FS-AC),
18
19 providing RF and DC signals. The RF signal was demodulated using an I & Q demodulator (Pulsar
20
21 Microwave, ID-10-412) to produce in-phase (I) and quadrature (Q) signals, which were low-pass
22
23 filtered (Minicircuits BLP-1.9+) and recorded by a digital storage oscilloscope (LeCroy, LT264,
24
25 350 MHz, 1 GSample s⁻¹). In the experiments reported here, the total acquisition timebase was 500
26
27 μ s, with a time-step of 200 ns. The DC signal from the detector was also recorded by the
28
29 oscilloscope to provide a monitor of the laser power as a function of wavelength.
30
31
32
33
34
35

36 The experiment was controlled by custom written Labview software. The oscilloscope was used
37
38 to average the I and Q waveforms over 250 valve shots for each probe laser wavelength, which
39
40 was stepped across the transition in intervals of ~ 100 MHz, with typically between 60 and 80
41
42 wavelength points recorded for each scan. Measurements were made in the following sequence, to
43
44 provide reliable relative signal sizes for different rotational states measured on different days. First,
45
46 a measurement of the incident molecular beam only was made, probing $j = 0.5$ via the $R_1(0.5)$
47
48 transition with the wheel/bath assembly retracted from the probe region. For selected rotational
49
50 states in the range $j = 4.5$ to 14.5 separate measurements were then made with the wheel/bath
51
52 assembly both retracted from, and inserted into, the probe region. The order in which these ‘wheel
53
54
55
56
57
58
59
60

1
2
3 out' and 'wheel in' measurements were made was alternated, and different final states were
4 measured in a random sequence. The 'wheel out' measurements provided a background
5 measurement of the small amount of CN present in the molecular beam in these higher rotational
6 states. No significant population was observed in the molecular beam for $j \geq 14.5$, and for these
7 states only the 'wheel in' or scattering measurements were made. After each pair of scattering and
8 background measurements were made, the wheel/bath assembly was retracted again and the cycle
9 restarted with another measurement of the incident beam $j = 0.5$ state. To ensure that scattering
10 only came from the coated region of the wheel, and not from the bath surface, additional
11 measurements were made with the wheel/bath assembly inserted, but with the wheel itself
12 removed. No measurable scattering was observed with this arrangement, providing confidence that
13 the scattering observed arises solely from the presence of the liquid-coated wheel.
14
15
16
17
18
19
20
21
22
23
24
25
26
27
28
29
30



31
32
33
34
35
36
37
38
39
40
41
42
43
44
45
46 **Figure 1.** A schematic representation of the experimental apparatus, with the DC electric discharge
47 molecular beam source in blue, the rotating wheel liquid surface assembly in green, and the in-
48 vacuum Herriott cell in magenta.
49
50
51
52
53
54
55
56
57
58
59
60

DATA ANALYSIS

The data consisted of I and Q signals as a function of time after the HV discharge trigger, together with the average probe laser power, for each wavelength. The first step in the data analysis was rotation of the I and Q signals by the overall experimental phase angle, to yield absorption (A) and dispersion (D) signals. The phase angle was determined independently using the well-established self-consistent methodology of North and Hall.³⁶ The A and D signals were then normalized at each wavelength by the average probe laser power. The x-axis was linearized in frequency using the simultaneously acquired monitor-etalon information, converted to Doppler shift in ms^{-1} . The line center was determined by finding the positions of the positive and negative peaks of the FM absorption signal, from a line shape averaged over the entire observed signal time, with the x-axis truncated to $\pm 2000 \text{ ms}^{-1}$. When processing both scattering and background measurements, FM Doppler line shapes for sequential $2 \mu\text{s}$ averages of the A and D signals were then constructed, with the baseline established using a pre-signal gate. The A and D FM Doppler lineshapes were simultaneously fitted, to determine the speed distribution of the CN radicals along the probe laser beam propagation direction, and thereby perpendicular to the molecular-beam axis and surface normal. The fitting process has been previously described in detail, with an assumed speed distribution used to simulate FM absorption and dispersion line shapes, including the appropriate linestrength for the probe transition. A simplex minimization was then applied to find the best fit speed distribution.^{43, 45} The integral of the speed distribution for each $2 \mu\text{s}$ average was then used to determine the relative population as a function of delay, which we refer to as an appearance profile. The measurements of the incident molecular beam via the $j = 0.5$ state were averaged over the entire delay for which signal was observed, from 130 to 250 μs . The single resulting A and D profiles were fitted as described above and integrated to yield a single number

1
2
3 quantifying the incident beam population. The average of incident-beam measurements made
4 immediately before and after the scattering and background measurements was used to normalize
5 these to day-to-day fluctuations in the performance of the CN-radical-discharge source.
6
7
8
9
10
11
12
13

14 RESULTS

15 16 17 18 **A. Characterization of incident $\text{CN}(X^2\Sigma^+)$ molecular beam**

19
20
21 Molecular-beam sources of $\text{CN}(X^2\Sigma^+)$ have been reported previously, and have been
22 subsequently applied to crossed molecular-beam scattering dynamics experiments. These sources
23 have used either photodissociation of a suitable precursor (e.g. BrCN or C_2N_2),⁵³⁻⁵⁴ or
24 photoablation of a graphite rod to form C atoms followed by reaction with N_2 ,⁵⁵ to generate CN
25 radicals that were subsequently entrained and cooled in a supersonic expansion to form a molecular
26 beam. To the best of our knowledge, there are no previous reports of the use of a DC electric
27 discharge to generate the CN radicals for subsequent entrainment and cooling.
28
29
30
31
32
33
34
35
36
37

38 Figure 2(a) shows appearance profiles for CN rotational states in the range $j = 0.5$ to 14.5, with
39 the relative signal sizes directly reflecting the relative populations in the different states, where the
40 error bars are 1σ standard error of the mean from 3 independent measurements. In each case, the
41 signal rises rapidly to a peak, before decaying more slowly to zero. The 10% to 90% rise time for
42 $j = 0.5$ is 7 μs , comparable to the 10 μs discharge pulse length, supporting the idea that this (as
43 expected) reflects the on-axis leading edge of the CN packet intersecting the probe laser. The
44 falling edge is slower, and for $j = 0.5$ displays a clear shoulder at $\approx 175 - 185 \mu\text{s}$. Since the
45 molecular beam is not skimmed, we cannot directly convert the appearance profile into an on-axis
46
47
48
49
50
51
52
53
54
55
56
57
58
59
60

1
2
3 speed distribution, as the shape of the falling edge will be a convolution of the speed distribution
4 with the angular spread of the molecular beam. Doppler lineshapes recorded at different delays
5 can be fitted to determine the transverse speed distributions, which indicate variations in the
6 angular distribution in the expansion associated with the observed shoulder in the appearance
7 profile (see Supporting Information). The time at which the peak signal appears after the discharge
8 pulse, 156 μs , corresponds to a CN speed of $1.90 \times 10^3 \text{ ms}^{-1}$. This is faster than the thermodynamic
9 prediction for a 100% He expansion from a room-temperature reservoir (ca. $1.75 \times 10^3 \text{ ms}^{-1}$). In
10 experiments using an identical discharge source that generated OD from the dissociation of D_2O
11 seeded in He, we measured an OD molecular beam speed of $1.81 \times 10^3 \text{ ms}^{-1}$.¹⁶ It therefore appears
12 that the molecular beams generated from discharge sources of this design are modestly faster than
13 conventional molecular beams from room-temperature reservoirs, consistent with additional
14 heating of the source gas within the discharge volume by the applied current. Considering the
15 entire appearance profile, the average kinetic energy of the CN molecular beam along the surface
16 normal is 43.5 kJ mol^{-1} . The total populations in different rotational levels in the f_1 spin-rotation
17 manifold, relative to the population of the $j = 0.5$ level, are shown in Figure 2(b). The lowest
18 rotational level, $j = 0.5$, is the most populated level, with a steady decline in population with
19 increasing j , indicating that a substantial degree of rotational cooling has occurred in the post-
20 discharge expansion. The distribution does not fit to a single rotational temperature, but does fit
21 well to a weighted 2-temperature distribution (Equation 1), shown as a logarithmic plot in the inset
22 to Figure 2(b).

$$\frac{P(j)}{(2j+1)} = C \left[\left(\frac{\alpha}{T_1} \right) e^{-\frac{E_{\text{rot}}(j)}{k_B T_1}} + \left(\frac{1-\alpha}{T_2} \right) e^{-\frac{E_{\text{rot}}(j)}{k_B T_2}} \right] \quad (1)$$

Here $P(j)$ is the relative population of level j , with rotational energy $E_{\text{rot}}(j)$, T_1 and T_2 are the rotational temperatures, α is the fraction at temperature T_1 , and C is an arbitrary overall scaling parameter. The results of this fit are displayed in Table 1, demonstrating that the majority of the rotational distribution is well described by a < 10 K temperature, with a minor component that is warmer, but still substantially below room temperature.

Table 1. Values of T_1 , T_2 and α obtained in a 2-temperature Boltzmann fit to the incident beam rotational populations. Confidence intervals are 1σ standard errors.

T_1 / K	T_2 / K	α
6.0 ± 0.8	127 ± 13	0.70 ± 0.05

This confirms that the DC electric discharge demonstrated here produces a rotationally cold supersonic molecular beam of CN(X) radicals, without the additional expense and experimental complexity required by the introduction of a photolysis or ablation laser.

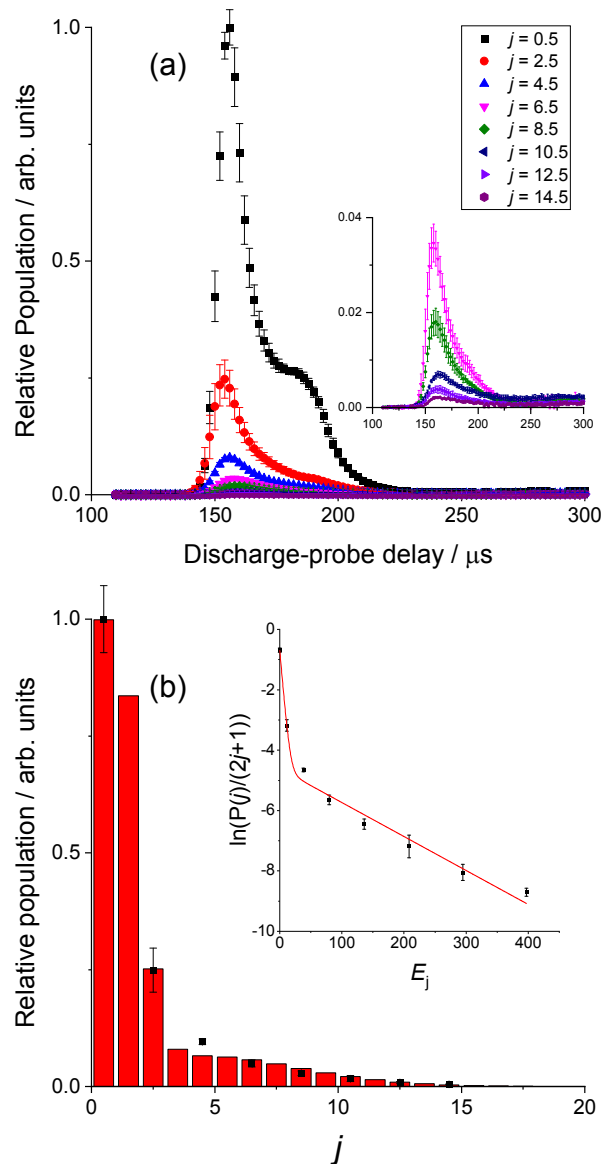
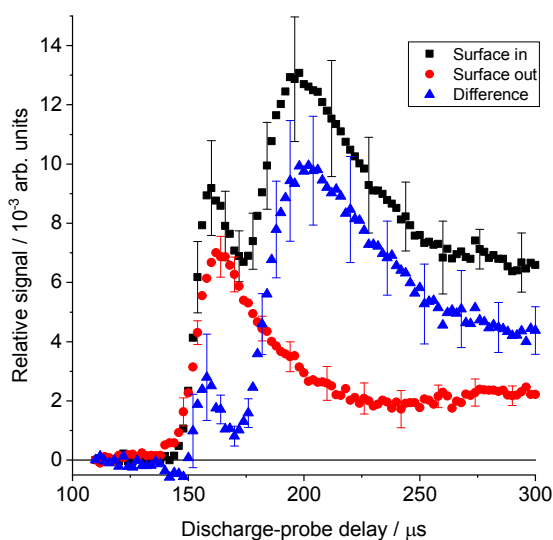


Figure 2. (a) Appearance profiles for the incident molecular beam for selected CN rotational levels, $j = 0.5$ to 14.5. (Inset) Expanded y-axis version of (a) showing appearance profiles for $j = 6.5$ to 14.5. (b) Relative rotational populations for selected rotational levels, $j = 0.5$ to 14.5, in the molecular beam. Experimental (black squares) and rotational distribution from the 2-temperature fit (red bars). (Inset) Two-temperature logarithmic fit of Equation 1 to the rotational populations in (b) to extract T_1 , T_2 and α as presented in Table 1.

B. Inelastic Scattering of $\text{CN}(X^2\Sigma^+)$ from a PFPE Surface

Figure 3 presents appearance profiles for $j = 10.5$, chosen as a representative sample from the complete data set, recorded with both the liquid surface present and with the surface retracted, and the difference of the two. In each case, the appearance profile is the average of three independent measurements acquired on different days, with normalization to the incident CN molecular beam population as discussed in the data analysis section above. A small signal is observed for the incident beam with the liquid surface retracted, peaking at 160 μs discharge-probe delay. This signal reaches a minimum at around 240 μs , and remains essentially constant until the end of the acquired time period (300 μs), consistent with off-axis paths observed in the free-jet expansion for this low-population rotationally excited state. When the liquid surface is introduced, a slightly larger initial peak at 160 μs is observed, followed by a local minimum, and then at $\approx 200 \mu\text{s}$ by an even larger signal, which then decays at long times. The early peak cannot be the result of direct scattering of CN from the liquid surface, as there is insufficient time for the CN to reach the surface and rebound to the probe region, resulting in an $\approx 40 \text{ mm}$ round trip. We believe that the increased early-time signal with the surface present is the result of gas-phase scattering. A relatively short temporal packet of CN radicals ($\approx 20 \mu\text{s}$ full width at half maximum) is embedded within a longer ($\approx 250 \mu\text{s}$) gas pulse. There is therefore time for the leading edge of the gas pulse, which is of course overwhelmingly composed of He, to strike the liquid surface and rebound into the path of the CN packet. Inelastic scattering with small positive Δj can then transfer some population from the highly populated low- j (≤ 4.5) levels up into the intermediate-to-high- j levels. We have observed similar behavior in previous interfacial scattering experiments in our laboratory involving OH radicals generated in a pulsed DC discharge.¹⁶ Consistent with this explanation, the

1
2
3 $j \leq 4.5$ levels display a negative difference around this time delay, while higher levels display
4 successively smaller early peaks. Previous studies of gas-phase inelastic scattering of $\text{CN}(X^2\Sigma^+)$
5 with He are also consistent with this picture, in which small Δj transfers are associated with strong
6 forward scattering and low translational energy transfer, maintaining the incident molecular beam
7 speed while redistributing some of the population across low- j levels.⁴³ We minimized this effect
8 by triggering the discharge as early as possible within the molecular beam pulse while still
9 maintaining discharge stability, as well as optimizing the valve-surface distance and consequent
10 molecular-beam density at the liquid surface.
11
12
13
14
15
16
17
18
19
20
21
22
23

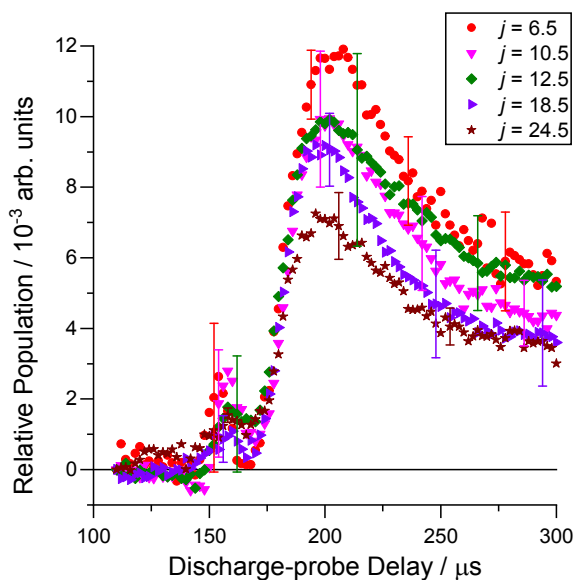


24
25
26
27
28
29
30
31
32
33
34
35
36
37
38
39
40
41
42
43
44 **Figure 3.** Appearance profiles for $j = 10.5$, with the liquid surface retracted (red circles) and
45 inserted (black squares), and the difference of these (blue triangles). Error bars represent 1σ
46 standard error of the mean of three independent measurements.
47
48
49

50
51 The large secondary peak, centered around $200 \mu\text{s}$, is only present when the surface is inserted,
52 and is consistent with a returning wave of CN radicals that have undergone inelastic scattering at
53
54
55
56
57
58
59
60

1
2
3 the liquid surface reaching the probe region. This returning signal can, of course, be larger than
4 the incident molecular beam signal for this rotational level as a consequence of translation to
5 the incident molecular beam signal for this rotational level as a consequence of translation to
6 rotational energy transfer at the liquid surface populating this level from the more highly populated
7 low- j levels in the incident beam. This observation and its interpretation is consistent with our
8 previous inelastic scattering experiments using LIF probing.^{9, 16-17, 34}
9
10
11
12
13
14
15

16 In Figure 4 we show appearance profiles for selected final states in the f_1 spin-rotation manifold,
17 $j = 6.5, 10.5, 12.5, 18.5,$ and 24.5 , relative to the population of the incident $j = 0.5$ level shown in
18 Figure 2(a). For $j = 6.5$ to 12.5 , these are differences of surface present and surface retracted,
19 however for $j = 18.5$ and 24.5 the incident beam intensity was negligible, and only the surface
20 present signal is presented. Clear differences in the overall signal sizes are observed, consistent
21 with varying rotational populations in the different final states. The rising edges of the appearance
22 profiles, and the peak times, are very similar for all final states. Differences are observed in the
23 falling edge of the profiles, although no clear trend with final- j is apparent.
24
25
26
27
28
29
30
31
32
33
34
35



1
2
3 **Figure 4.** Appearance profiles for CN($X^2\Sigma^+$) inelastically scattered from PFPE, for selected final
4 rotational levels, j . Populations are relative to that from the incident $j = 0.5$ level. Selected error
5 bars are 1 standard error of the mean of 3 independent measurements on different days. For $j \leq$
6 12.5 the profile is the difference of surface present and retracted, for $j = 18.5$ and 24.5 the profile
7 is surface present only.
8
9
10
11
12
13
14

15 The relative rotational populations derived from integrating the appearance profiles in the delay
16 range 176 – 266 μs are shown in Figure 5. We have excluded signals after 266 μs to ensure that
17 the rotational populations are not modified by secondary gas-phase collisions. It is difficult to
18 determine the pressure in the probe region at the experimental measurement time. A typical
19 centerline pressure for a pulsed molecular beam is of order 1 mTorr. Assuming a gas kinetic rate
20 constant typical for rotational energy transfer ($10^7 \text{ Torr}^{-1} \text{ s}^{-1}$), at this pressure the CN would
21 undergo a collision every 100 μs . However, the surface-scattered CN and He are expanding into
22 an evacuated chamber ($1 \times 10^{-5} \text{ mbar}$), implying that the average probe region pressure is
23 substantially less than 1 mTorr during this experimental measurement time, and that accordingly
24 the nascent rotational distributions from surface scattering are not substantially modified by
25 subsequent gas-phase collisions. We note that in principle the signals should be corrected for flux-
26 density effects, as the absorption probe method measures the instantaneous density in the probe
27 beam, which necessarily depends on the speed of the scattered CN. However, as in our previous
28 experiments studying OH inelastic collisions using LIF, providing an appropriate correction to
29 convert this density to a flux is challenging, given the unknown details of the scattering angle
30 distribution and its interaction with the (multi-beam) probe laser geometry.¹⁶ Given the similar
31 shapes of the appearance profiles in the integrated time-window, we have assumed that the
32 appropriate density-flux correction will have similar effects on the different rotational levels, and
33
34
35
36
37
38
39
40
41
42
43
44
45
46
47
48
49
50
51
52
53
54
55
56
57
58
59
60

1
2
3 accordingly present rotational populations without correction. Figure 5(a) displays a Boltzmann
4 plot of the rotational populations and the associated linear fit which yields a rotational temperature,
5
6 $T_R = 850 \pm 130$ K. No significant improvement in the quality of the fit was found when fitting to
7
8 a two-temperature model, as given by Equation 1. Figure 5(b) shows the relative rotational
9
10 populations as a function of j , together with a simulation for $T_R = 850$ K normalized to have the
11
12 same total population among the observed levels.
13
14
15
16
17
18
19
20
21
22
23
24
25
26
27
28
29
30
31
32
33
34
35
36
37
38
39
40
41
42
43
44
45
46
47
48
49
50
51
52
53
54
55
56
57
58
59
60

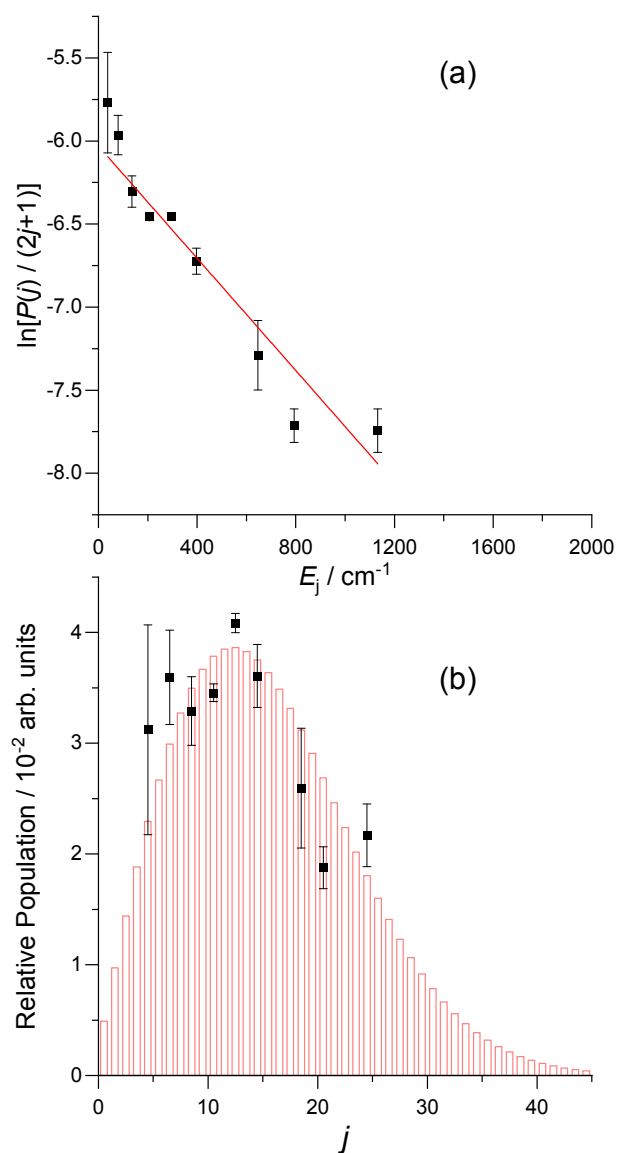


Figure 5. (a) Boltzmann plot for $\text{CN}(X^2\Sigma^+)$ scattered from the PFPE surface, spanning rotational levels in the f_1 spin-rotation manifold ranging from $j = 4.5$ to $j = 24.5$, together with the linear best fit. Error bars are 1σ standard error of the mean from 3 independent measurements. (b) Rotational populations, relative to that for the incident $j = 0.5$ level. Experiment (black squares), simulation assuming $T_R = 850$ K from the linear fit in (a) (red bars).

1
2
3 Figure 6(a) shows FM Doppler absorption lineshapes for CN inelastically scattered into $j = 6.5$,
4 summed over three selected time periods which we define as: rising edge (176 – 191.8 μs); peak
5 (192 – 223.8 μs); and falling edge (224 - 266 μs). The results of fitting to extract the speed
6 distribution are shown, as well as a simulation of a 298 K Gaussian Doppler lineshape, appropriate
7 for a thermalized gas-phase velocity distribution. All three scattered Doppler lineshapes are
8 significantly wider than the thermal lineshape, indicating translational temperatures perpendicular
9 to the surface that are greater than 298 K. The width of the lineshapes clearly decreases from the
10 rising edge to the falling edge, demonstrating that the early-appearance-time CN has a higher
11 transverse translational energy. This trend is reproduced for all final product states probed (see the
12 Supporting Information). The transverse speed distributions for these different delays, extracted
13 from the fits in Figure 6(a), are presented in Figure 6(b), together with a Maxwell-Boltzmann
14 distribution for 298 K. Consistent with the observed Doppler lineshapes, the transverse speed
15 distributions for all of the measured delays peak at substantially higher speeds than the 298 K
16 Maxwell-Boltzmann distribution, with most probable speeds of 830, 750 and 670 ms^{-1} for the
17 rising edge, peak and falling edge delays, respectively, while the most probable speed for the 298
18 K Maxwell-Boltzmann is 436 ms^{-1} . The shapes of the fitted transverse speed distributions are also
19 inconsistent with Maxwell-Boltzmann distributions, a feature particularly noticeable for the rising-
20 edge delay, where the transverse speed distribution displays sharper curvature on the fast side than
21 the slow, i.e. the opposite of a Maxwell-Boltzmann. This non-Boltzmann behavior is directly
22 reflected in the observed Doppler lineshapes, and attempts to fit these to Gaussian lineshapes (the
23 one-dimensional Doppler projection of a Maxwell-Boltzmann distribution) varying the
24 translational temperature were unsuccessful, confirming that the lineshapes are significantly non-
25 Gaussian.
26
27
28
29
30
31
32
33
34
35
36
37
38
39
40
41
42
43
44
45
46
47
48
49
50
51
52
53
54
55
56
57
58
59
60

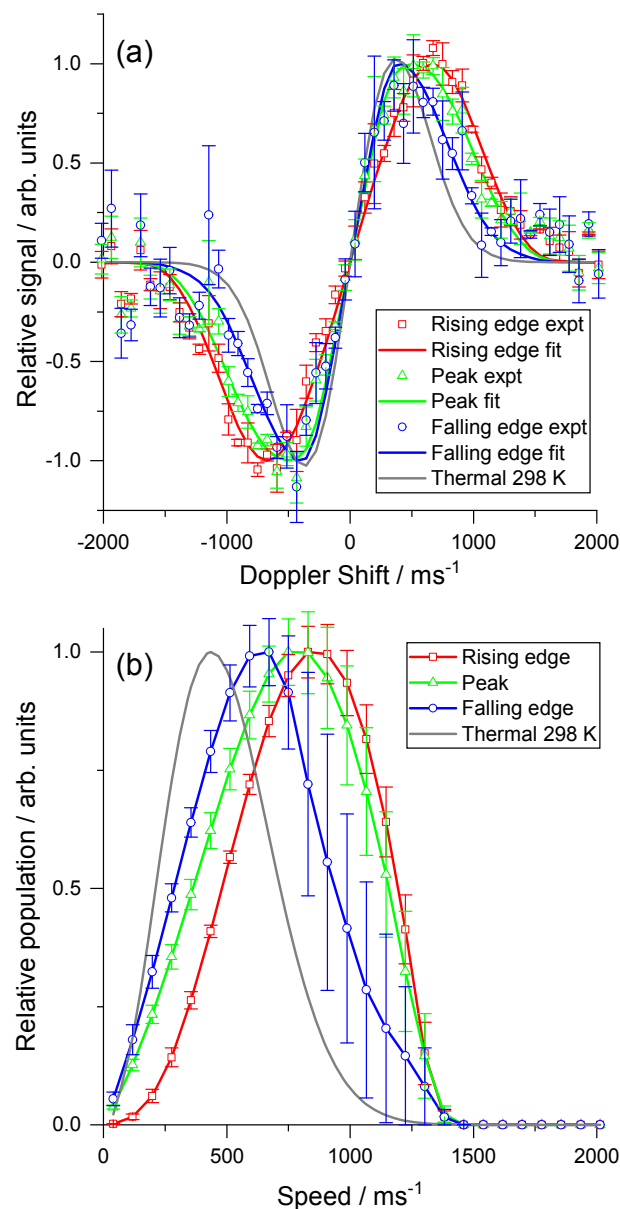


Figure 6. (a) FM absorption Doppler lineshapes for $j = 6.5$, integrated over rising edge, peak and falling edge delays. Rising edge data (red open squares) and fit to determine the translational energy distribution (red solid line), peak data (green open triangles) and fit (green solid line), falling edge data (blue open circles) and fit (blue solid line). Simulation of FM Doppler lineshape for 298 K Maxwell-Boltzmann speed distribution (grey solid line). (b) Speed distributions extracted from the fits to data shown in (a). Rising edge (red squares and line), peak (green

1
2
3 triangles and line), falling edge (blue circles and line) and a 298 K Maxwell-Boltzmann
4
5 distribution (grey line).
6
7
8
9

10 **DISCUSSION**

11
12 We first discuss the measured rotational distribution for the scattered CN. It is immediately
13 obvious that the scattered CN is rotationally excited relative to the incident molecular beam
14 distribution. The scattered distribution is reasonably well-described by a Boltzmann distribution
15 with a temperature, $T_R = 850$ K, which is substantially above that of the surface, $T_S = 298$ K. It is
16 very common in surface-scattering experiments to analyze the observed scattering by comparison
17 to two limiting cases. The first is *thermal desorption* (TD), where the incident species has fully
18 accommodated with the surface before desorption. A TD sample will therefore display a rotational
19 distribution reflecting the surface temperature, as well as a Maxwell-Boltzmann speed distribution
20 similarly defined by T_S . The dramatically higher rotational temperature observed here suggests
21 that there is at most a modest component of TD scattering in this system. By definition, the
22 remaining fraction of the scattering that is not TD is described as *impulsive scattering* (IS), in
23 which the incident species has undergone one or potentially a small number of collisions with the
24 surface, but has not fully equilibrated with it. There is no *a priori* reason why the rotational
25 distribution from a direct scattering process should be described by a rotational temperature, but
26 recent experiments studying a range of molecular species with a wide variety of liquid surfaces
27 have shown that this is a very common outcome.^{9, 16-19, 21-22, 24, 27-31, 34, 56} The fitted rotational
28 temperature corresponds to a fraction $f_R = 0.16 \pm 0.02$ of the available incident kinetic energy being
29 converted from translation to rotation in collisions at the liquid surface. This is broadly comparable
30 to the previous limited measurements of rotationally inelastic scattering of small molecules at
31
32
33
34
35
36
37
38
39
40
41
42
43
44
45
46
47
48
49
50
51
52
53
54
55
56
57
58
59
60

1
2
3 PFPE surfaces. In our own previous work using LIF to study OD inelastic scattering at a PFPE
4 surface, using a molecular beam source at normal incidence and a laboratory frame kinetic energy
5 of 30 kJ mol⁻¹, we found $f_R = 0.11$.¹⁶ Nesbitt and co-workers have studied both CO₂ and NO
6 collisions with PFPE. In both cases, the product rotational distributions can be fitted to a two-
7 temperature IS:TD model. Considering the IS components alone, $f_R = 0.14$ and 0.12 for CO₂ and
8 NO, respectively, at incident kinetic energies of 44 and 84 kJ mol⁻¹.^{22, 31} In contrast to the work of
9 Nesbitt and co-workers, but consistent with our own previous work on OH inelastic scattering, we
10 see no strong evidence for a TD component in the rotational distribution within the limitations of
11 the measured signal-to-noise ratio, and therefore conclude that the rotational distribution is
12 dominated by impulsive scattering.
13
14
15
16
17
18
19
20
21
22
23
24
25

26 We now consider the translational energy of the scattered CN. There are two sources of
27 information for this: the shapes of the appearance profiles and the Doppler lineshapes. The delay
28 between the peaks of the incident CN and scattered CN appearance profiles is essentially
29 independent of the final rotational state at ≈ 40 μ s. The probe beams are centered 20 mm from the
30 liquid surface, and the measured incident beam speed of 1.9×10^3 ms⁻¹ implies a flight time of \approx
31 10 μ s to the surface. The remaining ≈ 30 μ s delay is consistent with a scattered speed at the peak
32 of the return signal of ≈ 650 ms⁻¹. This is faster than the most probable speed for a 298 K thermal
33 distribution, 436 ms⁻¹, consistent with the general conclusion from the rotational distribution that
34 the majority of the scattering is impulsive in nature. At face value, this corresponds to an
35 approximate translational temperature of ≈ 670 K, comparable to but somewhat lower than the
36 rotational temperature. However, caution should be exercised in relating the appearance profiles
37 quantitatively to the scattered speed distribution in such a simple way. The return flight path, and
38 hence return time-of-flight, is short compared to the incident packet width. This results in the
39
40
41
42
43
44
45
46
47
48
49
50
51
52
53
54
55
56
57
58
59
60

1
2
3 scattered appearance profile being strongly convoluted by the incident packet width. The probe
4 region is also ≈ 8 mm in diameter, a significant fraction of the average 20 mm flight path from the
5 surface. Most importantly, the scattered CN may be detected anywhere along any of the 14 probe
6 beam paths in the Herriott cell, including locations which are some distance from the central axis
7 of the incident molecular beam along the direction of laser-beam propagation. The actual flight
8 paths from the surface to the probe beam that contribute to the observed appearance profile will
9 therefore sample a wide range of product scattering angles, arising from collisions with the liquid
10 surface across the width of the wheel upon which the initial CN beam was incident. There is no
11 simple way to deconvolute these various effects. Monte-Carlo simulation can, in principle, be used
12 to forward-simulate appearance profiles based on assumed scattering distributions, as
13 demonstrated in some of our previous work using LIF as a probe method, although we have not
14 attempted that yet here.^{9, 16}

15
16
17
18
19
20
21
22
23
24
25
26
27
28
29
30
31 More straightforwardly, the transverse Doppler lineshapes do provide unambiguous information
32 on a component of the scattered CN velocities. The transverse speed distributions extracted from
33 the lineshapes provide clear evidence of impulsive scattering, being substantially faster than a 298
34 K thermal distribution. The most probable transverse speeds are 830, 750 and 670 ms^{-1} for the
35 rising edge, peak and falling edge delays, corresponding to average kinetic energies of 10.2, 8.8,
36 and 6.7 kJ mol^{-1} , respectively. This variation within the appearance profile is self-consistent with
37 the speeds normal and transverse to the surface being correlated, and the simplest interpretation of
38 the appearance profile as a (somewhat convoluted) time-of-flight measurement. Interestingly, no
39 strong evidence for a substantial thermalized component of transverse speeds is observed even for
40 the lower rotational levels, where it would be expected to make the largest contribution. It might
41 hypothetically be possible to associate the slower transverse speeds with a TD component and the
42
43
44
45
46
47
48
49
50
51
52
53
54
55
56
57
58
59
60

1
2
3 residual with an IS mechanism, but with no observable bimodality in the speed distribution there
4
5 is no clear justification for attempting such an analysis. This is consistent with what we have
6
7 concluded above about the absence of a substantial TD component in the rotational distributions,
8
9 within the current signal-to-noise level and finite number of probed rotational levels.
10
11

12 We have previously observed broadly similar behavior in inelastic scattering of OD from PFPE
13
14 surfaces, with scattered OD speeds that are superthermal and do not display any clear surface-
15
16 temperature thermal component.¹⁷ In contrast, the scattered speed distributions of both NO and
17
18 CO₂ from PFPE observed by Nesbitt and co-workers have been successfully interpreted within an
19
20 IS:TD model, with substantial thermal components at the surface temperature, consistent with their
21
22 associated rotational temperature analysis.^{18-19, 21-22, 24, 27, 31} The origin of these implied differences
23
24 in the fraction of the scattered distribution that appears to be surface equilibrated is as yet unknown.
25
26 Further work is clearly required, including improvements in signal-to-noise and an expansion of
27
28 the present study to include different incident kinetic energies, better-defined initial transverse
29
30 velocity distributions through skimming of the molecular beam, and the introduction of different
31
32 liquid surfaces, particularly potentially reactive hydrocarbon surfaces such as squalane, C₃₀H₆₂.
33
34
35
36
37
38
39

40 CONCLUSION

41
42 We have reported the first application of frequency-modulation absorption spectroscopy as a
43
44 probe of gas-liquid interfacial scattering, including the first use of a DC electric discharge source
45
46 to generate a pulsed rotationally cold molecular beam of CN radicals. The rotationally inelastic
47
48 scattering of CN radicals at the surface of PFPE is dominated by impulsive scattering, as concluded
49
50 both from the extended rotational distributions and the non-Gaussian, superthermal transverse-
51
52 speed distributions. There is no clear evidence, within the current signal-to-noise, of bimodality in
53
54
55
56
57
58
59
60

1
2
3 either of these distributions and hence no need to invoke a discrete thermalized component to
4 explain the observations. Overall, around 15% of the incident kinetic energy is converted into
5 rotation, comparable amounts into translation, with the remainder lost into the (unobserved)
6 motions of the PFPE. This study demonstrates the utility of FM-absorption spectroscopy as a
7 sensitive probe of gas-liquid interfacial scattering, and extends the (limited) range of molecular
8 species for which quantum-state resolved scattering information at liquid surfaces is available.
9
10
11
12
13
14
15
16
17
18
19
20

21 ASSOCIATED CONTENT

22
23 **Supporting Information.** Figure S1 showing Doppler lineshapes as a function of discharge-
24 probe delay for the incident molecular beam, and resulting transverse speed distributions. Figure
25 S2 showing Doppler lineshapes for rising edge, peak and falling edge delays for three
26 representative rotational levels $j = 6.5, 12.5$ and 18.5 .
27
28
29
30
31
32
33

34 AUTHOR INFORMATION

35 36 **Corresponding Author**

37
38
39 *E-mail: m.l.costen@hw.ac.uk
40
41

42 43 **Notes**

44
45 The authors declare no competing financial interest.
46
47

48 49 **ACKNOWLEDGMENT**

50
51 The authors acknowledge financial support from the EPSRC (EP/M021823/1 and EP/P001459/1)
52 and Heriot-Watt University (James Watt Scholarship for K.E.M.). We thank Dr D. Glowacki
53 (University of Bristol) for helpful discussions.
54
55
56
57
58
59
60

REFERENCES

1. Nathanson, G. M., Molecular beam studies of gas-liquid interfaces. *Annu Rev Phys Chem* **2004**, *55*, 231-255.
2. Tesa-Serrate, M. A.; Smoll, E. J.; Minton, T. K.; McKendrick, K. G., Atomic and Molecular Collisions at Liquid Surfaces. *Annu Rev Phys Chem* **2016**, *67*, 515-540.
3. Faust, J. A.; Nathanson, G. M., Microjets and coated wheels: versatile tools for exploring collisions and reactions at gas-liquid interfaces. *Chem Soc Rev* **2016**, *45*, 3609-3620.
4. Saecker, M. E.; Govoni, S. T.; Kowalski, D. V.; King, M. E.; Nathanson, G. M., Molecular-Beam Scattering from Liquid Surfaces. *Science* **1991**, *252*, 1421-1424.
5. Garton, D. J.; Minton, T. K.; Alagia, M.; Balucani, N.; Casavecchia, P.; Volpi, G. G., Reactive scattering of ground-state and electronically excited oxygen atoms on a liquid hydrocarbon surface. *Faraday Discuss* **1997**, *108*, 387-399.
6. Kenyon, A. J.; McCaffery, A. J.; Quintella, C. M.; Zidan, M. D., Investigation of Dynamical Processes at Liquid Surfaces by Molecular-Scattering. *J Chem Soc Faraday T* **1993**, *89*, 3877-3884.
7. Kenyon, A. J.; McCaffery, A. J.; Quintella, C. M.; Zidan, M. D., Dynamics of the Gas-Liquid Interface from Laser Molecular-Beam Scattering. *Faraday Discuss* **1993**, *96*, 245-254.
8. Kohler, S. P. K.; Allan, M.; Costen, M. L.; McKendrick, K. G., Direct gas-liquid interfacial dynamics: The reaction between O(³P) and a liquid hydrocarbon. *J Phys Chem B* **2006**, *110*, 2771-2776.
9. Bagot, P. A. J.; Waring, C.; Costen, M. L.; McKendrick, K. G., Dynamics of inelastic scattering of OH radicals from reactive and inert liquid surfaces. *J Phys Chem C* **2008**, *112*, 10868-10877.
10. Waring, C.; Bagot, P. A. J.; Bebbington, M. W. P.; Raisanen, M. T.; Buck, M.; Costen, M. L.; McKendrick, K. G., How Penetrable Are Thioalkyl Self-Assembled Monolayers? *J Phys Chem Lett* **2010**, *1*, 1917-1921.
11. Waring, C.; Bagot, P. A. J.; Slattery, J. M.; Costen, M. L.; McKendrick, K. G., O(³P) Atoms as a Probe of Surface Ordering in 1-Alkyl-3-methylimidazolium-Based Ionic Liquids. *J Phys Chem Lett* **2010**, *1*, 429-433.
12. McKendrick, K. G.; Waring, C.; King, K. L.; Costen, M. L., Dynamics of the Gas-Liquid Interfacial Reaction of O(¹D) with a Liquid Hydrocarbon. *J Phys Chem A* **2011**, *115*, 7210-7219.
13. Waring, C.; Bagot, P. A. J.; Costen, M. L.; McKendrick, K. G., Reactive Scattering as a Chemically Specific Analytical Probe of Liquid Surfaces. *J Phys Chem Lett* **2011**, *2*, 12-18.
14. Tesa-Serrate, M. A.; King, K. L.; Paterson, G.; Costen, M. L.; McKendrick, K. G., Site and bond-specific dynamics of reactions at the gas-liquid interface. *Phys Chem Chem Phys* **2014**, *16*, 173-183.
15. Bruce, D. W., et al., Nanosegregation and Structuring in the Bulk and at the Surface of Ionic-Liquid Mixtures. *J Phys Chem B* **2017**, *121*, 6002-6020.
16. Bianchini, R. H.; Tesa-Serrate, M. A.; Costen, M. L.; McKendrick, K. G., Collision-Energy Dependence of the Uptake of Hydroxyl Radicals at Atmospherically Relevant Liquid Surfaces. *J Phys Chem C* **2018**, *122*, 6648-6660.
17. Bianchini, R. H.; Roman, M. J.; Costen, M. L.; McKendrick, K. G., Real-space laser-induced fluorescence imaging applied to gas-liquid interfacial scattering. *J Chem Phys* **2019**, *151*, 054201.

18. Perkins, B. G.; Haber, T.; Nesbitt, D. J., Quantum state-resolved energy transfer dynamics at gas-liquid interfaces: IR laser studies of CO₂ scattering from perfluorinated liquids. *J Phys Chem B* **2005**, *109*, 16396-16405.
19. Perkins, B. G.; Nesbitt, D. J., Quantum-state-resolved CO₂ scattering dynamics at the gas-liquid interface: Incident collision energy and liquid dependence. *J Phys Chem B* **2006**, *110*, 17126-17137.
20. Zolot, A. M.; Harper, W. W.; Perkins, B. G.; Dagdigian, P. J.; Nesbitt, D. J., Quantum-state resolved reaction dynamics at the gas-liquid interface: Direct absorption detection of HF(v,J) product from F(²P) plus squalane. *J Chem Phys* **2006**, *125*, 021101.
21. Perkins, B. G.; Nesbitt, D. J., Quantum-state-resolved CO₂ scattering dynamics at the gas-liquid interface: Dependence on incident angle. *J Phys Chem A* **2007**, *111*, 7420-7430.
22. Perkins, B. G.; Nesbitt, D. J., Correlated angular and quantum state-resolved CO₂ scattering dynamics at the gas-liquid interface. *J Phys Chem A* **2008**, *112*, 9324-9335.
23. Perkins, B. G.; Nesbitt, D. J., Stereodynamics in state-resolved scattering at the gas-liquid interface. *P Natl Acad Sci USA* **2008**, *105*, 12684-12689.
24. Perkins, B. G.; Nesbitt, D. J., Quantum state-resolved CO₂ collisions at the gas-liquid interface: Surface temperature-dependent scattering dynamics. *J Phys Chem B* **2008**, *112*, 507-519.
25. Zolot, A. M.; Dagdigian, P. J.; Nesbitt, D. J., Quantum-state resolved reactive scattering at the gas-liquid interface: F plus squalane (C₃₀H₆₂) dynamics via high-resolution infrared absorption of nascent HF(v,J). *J Chem Phys* **2008**, *129*, 194705.
26. Perkins, B. G.; Nesbitt, D. J., Stereodynamics at the Gas-Liquid Interface: Orientation and Alignment of CO₂ Scattered from Perfluorinated Liquid Surfaces. *J Phys Chem A* **2010**, *114*, 1398-1410.
27. Perkins, B. G.; Nesbitt, D. J., High resolution Dopplerimetry of correlated angular and quantum state-resolved CO₂ scattering dynamics at the gas-liquid interface. *Phys Chem Chem Phys* **2010**, *12*, 14294-14308.
28. Ziemkiewich, M. P.; Zutz, A.; Nesbitt, D. J., Inelastic Scattering of Radicals at the Gas-Ionic Liquid Interface: Probing Surface Dynamics of BMIM-Cl, BMIM-BF₄, and BMIM-Tf₂N by Rovibronic Scattering of NO [²Π_{1/2}(0.5)]. *J Phys Chem C* **2012**, *116*, 14284-14294.
29. Zutz, A.; Nesbitt, D. J., Nonadiabatic Spin-Orbit Excitation Dynamics in Quantum-State-Resolved NO(²Π_{1/2}) Scattering at the Gas-Room Temperature Ionic Liquid Interface. *J Phys Chem C* **2015**, *119*, 8596-8607.
30. Zutz, A.; Nesbitt, D. J., Quantum state-resolved molecular scattering of NO (²Π_{1/2}) at the gas-[C_(n)mim][Tf₂N] room temperature ionic liquid interface: Dependence on alkyl chain length, collision energy, and temperature. *AIP Adv* **2016**, *6*, 105207.
31. Zutz, A.; Nesbitt, D. J., Angle-resolved molecular beam scattering of NO at the gas-liquid interface. *J Chem Phys* **2017**, *147*, 054704.
32. Zutz, A.; Nesbitt, D. J., Quantum-State-Resolved Scattering of NO(²Π_{1/2}) from Hot Molten Au(liq): On the Role of Thermal Electron-Hole Pairs in Vibrational Excitation Dynamics. *J Phys Chem C* **2018**, *122*, 17161-17169.
33. Ryazanov, M.; Nesbitt, D. J., Quantum-state-resolved studies of aqueous evaporation dynamics: NO ejection from a liquid water microjet. *J Chem Phys* **2019**, *150*, 044301.
34. Waring, C.; King, K. L.; Bagot, P. A. J.; Costen, M. L.; McKendrick, K. G., Collision dynamics and reactive uptake of OH radicals at liquid surfaces of atmospheric interest. *Phys Chem Chem Phys* **2011**, *13*, 8457-8469.

- 1
2
3 35. Bloch, J. C.; Field, R. W.; Hall, G. E.; Sears, T. J., Time-Resolved Frequency-
4 Modulation Spectroscopy of Photochemical Transients. *J Chem Phys* **1994**, *101*, 1717-1720.
5 36. Hall, G. E.; North, S. W., Transient laser frequency modulation spectroscopy. *Annu Rev*
6 *Phys Chem* **2000**, *51*, 243-274.
7 37. Costen, M. L.; North, S. W.; Hall, G. E., Vector signatures of adiabatic and diabatic
8 dynamics in the photodissociation of ICN. *J Chem Phys* **1999**, *111*, 6735-6749.
9 38. Costen, M. L.; Hall, G. E., Coherent and incoherent orientation and alignment of ICN
10 photoproducts. *Phys Chem Chem Phys* **2007**, *9*, 272-287.
11 39. North, S. W.; Fei, R. A.; Sears, T. J.; Hall, G. E., CN radical reaction rate measurements
12 by time-resolved FM spectroscopy. *Int J Chem Kinet* **1997**, *29*, 127-129.
13 40. Lockhart, J. P. A.; Gross, E. C.; Sears, T. J.; Hall, G. E., Kinetic study of the OH plus
14 ethylene reaction using frequency-modulated laser absorption spectroscopy. *Int J Chem Kinet*
15 **2019**, *51*, 412-421.
16 41. Komissarov, A. V.; Lin, A.; Sears, T. J.; Hall, G. E., State-resolved thermalization of
17 singlet and mixed singlet-triplet states of CH₂. *J Chem Phys* **2006**, *125*, 084308
18 42. Forthomme, D.; Hause, M. L.; Yu, H. G.; Dagdigian, P. J.; Sears, T. J.; Hall, G. E.,
19 Doppler-Resolved Kinetics of Saturation Recovery. *J Phys Chem A* **2015**, *119*, 7439-7450.
20 43. Alagappan, A.; Costen, M. L.; McKendrick, K. G., Frequency modulated spectroscopy as
21 a probe of molecular collision dynamics. *Spectrochim Acta A* **2006**, *63*, 910-922.
22 44. Alagappan, A.; Ballingall, I.; Costen, M. L.; McKendrick, K. G., Differential scattering
23 cross-sections for CN A²Π+Ar. *J Chem Phys* **2007**, *126*, 041103.
24 45. Alagappan, A.; Ballingall, I.; Costen, M. L.; McKendrick, K. G.; Paterson, G.,
25 Efficiencies of state and velocity-changing collisions of superthermal CN A²Π with He, Ar, N₂
26 and O₂. *Phys Chem Chem Phys* **2007**, *9*, 747-754.
27 46. Ballingall, I.; Rutherford, M. F.; McKendrick, K. G.; Costen, M. L., Elastic
28 depolarization and polarization transfer in CN(A²Π, v=4) + Ar collisions. *Mol Phys* **2010**, *108*,
29 847-863.
30 47. McGurk, S. J.; McKendrick, K. G.; Costen, M. L.; Bennett, D. I. G.; Klos, J.; Alexander,
31 M. H.; Dagdigian, P. J., Depolarization of rotational angular momentum in CN(A²Π, v = 4) + Ar
32 collisions. *J Chem Phys* **2012**, *136*, 164306-15.
33 48. McGurk, S. J.; McKendrick, K. G.; Costen, M. L.; Alexander, M. H.; Dagdigian, P. J.,
34 Parity-dependent oscillations in collisional polarization transfer: CN(A²Π, v = 4) + Ar. *J Chem*
35 *Phys* **2013**, *139*, 124304.
36 49. McGurk, S. J.; Halpern, J. B.; McKendrick, K. G.; Costen, M. L., Parity-Dependent
37 Rotational Energy Transfer in CN(A²Π, v=4, j F₁ ε) + N₂, O₂, and CO₂ Collisions. *J Phys Chem*
38 *A* **2014**, *118*, 2007-2017.
39 50. Halfmann, T.; Koensgen, J.; Bergmann, K., A source for a high-intensity pulsed beam of
40 metastable helium atoms. *Meas Sci Technol* **2000**, *11*, 1510-1514.
41 51. Herriott, D.; Kompfner, R.; Kogelnik, H., Off-Axis Paths in Spherical Mirror
42 Interferometers. *Appl Optics* **1964**, *3*, 523-526.
43 52. Kaur, D.; Desouza, A. M.; Wanna, J.; Hammad, S. A.; Mercorelli, L.; Perry, D. S.,
44 Multipass Cell for Molecular-Beam Absorption-Spectroscopy. *Appl Optics* **1990**, *29*, 119-124.
45 53. Huang, C.; Li, W.; Estillore, A. D.; Suits, A. G., Dynamics of CN plus alkane reactions
46 by crossed-beam dc slice imaging. *J Chem Phys* **2008**, *129*, 074301.
47
48
49
50
51
52
53
54
55
56
57
58
59
60

- 1
2
3 54. Lai, L. H.; Wang, J. H.; Che, D. C.; Liu, K. P., Direct mapping of vibrational-specific
4 angular distributions of the polyatomic reaction product: $\text{CN} + \text{D}_2 \rightarrow \text{DCN} + \text{D}$. *J Chem Phys* **1996**,
5 *105*, 3332-3335.
6
7 55. Kaiser, R. I.; Ting, J. W.; Huang, L. C. L.; Balucani, N.; Asvany, O.; Lee, Y. T.; Chan,
8 H.; Stranges, D.; Gee, D., A versatile source to produce high-intensity, pulsed supersonic radical
9 beams for crossed-beam experiments: The cyanogen radical $\text{CN}(X^2\Sigma^+)$ as a case study. *Rev Sci*
10 *Instrum* **1999**, *70*, 4185-4191.
11 56. Livingston Large, T. A.; Nesbitt, D. J., Quantum State and Doppler-Resolved Scattering
12 of Thermal/Hyperthermal DCl at the Gas-Liquid Interface: Support for a Simple “Lever Arm”
13 Model of the Energy-Transfer Dynamics. *J Phys Chem C* **2019**, *123*, 3449-3460.
14
15
16
17
18
19
20
21
22
23
24
25
26
27
28
29
30
31
32
33
34
35
36
37
38
39
40
41
42
43
44
45
46
47
48
49
50
51
52
53
54
55
56
57
58
59
60

Table of contents graphic

